



ELSEVIER

Available online at www.sciencedirect.com

jmr&t
Journal of Materials Research and Technology

journal homepage: www.elsevier.com/locate/jmrt



Original Article

Exploring the industrial implementation of W–S–N coatings: a detailed study of the synthesis, compositional, structural, mechanical and multi-environment lubrication properties



Talha Bin Yaqub ^{a,b}, Abbas Al-Rjoub ^a, Albano Cavaleiro ^{a,b},
Filipe Fernandes ^{a,b,*}

^a University of Coimbra, CEMMPRE - Centre for Mechanical Engineering Materials and Processes, Department of Mechanical Engineering, Rua Luís Reis Santos, 3030-788, Coimbra, Portugal

^b IPN - LED & MAT - Instituto Pedro Nunes, Laboratory of Tests, Wear and Materials, Rua Pedro Nunes, 3030-199, Coimbra, Portugal

ARTICLE INFO

Article history:

Received 27 December 2021

Accepted 23 February 2022

Available online 26 February 2022

Keywords:

W–S–N coatings

Industrial solid lubricant coatings

Low friction

Diverse environment tribology

Transition metal dichalcogenides

ABSTRACT

The work presents a detailed analysis of the synthesis, compositional, morphological, structural, mechanical and diverse atmosphere sliding characteristics of reactive sputtered W–S–N coatings. The aim is to perform an organized study to explore the sliding performance in three different environments (room temperature, 200 °C and dry N₂) and disseminate the results to promote the application of TMD-N coatings for actual industrial implementation. All coatings are sub-stoichiometric in sulphur with respect to WS₂ phase. The coatings show highly compact morphologies, as compared to the literature results. The pure WS_x coating has (100) preferential orientation. However, the N-alloyed ones display strong (002) preferential orientation which is usually linked to a high sliding efficiency. The pure and W/S/N coatings exhibit a maximum hardness values of 3.7 GPa and 8.0 GPa, respectively. The minimum friction coefficient and wear rates observed for W–S–N coatings in room temperature, 200 °C and dry N₂ are 0.09 vs. 7.2 × 10⁻⁸ mm³/Nm, 0.02 vs. 7.1 × 10⁻⁸ mm³/Nm and 0.03 vs. 9.3 × 10⁻⁹ mm³/Nm, respectively. On the other hand, the sliding properties at room temperature are comparable to the literature for both TMD-N and TMD-C coatings.

© 2022 The Authors. Published by Elsevier B.V. This is an open access article under the CC BY-NC-ND license (<http://creativecommons.org/licenses/by-nc-nd/4.0/>).

* Corresponding author.

E-mail address: filipe.fernandes@dem.uc.pt (F. Fernandes).

<https://doi.org/10.1016/j.jmrt.2022.02.116>

2238-7854/© 2022 The Authors. Published by Elsevier B.V. This is an open access article under the CC BY-NC-ND license (<http://creativecommons.org/licenses/by-nc-nd/4.0/>).

1. Introduction

Solid lubrication has emerged as a dominant research field in the past few decades. Among various low friction thin coatings, transition metal dichalcogenides (TMDs) share a major research domain. Nevertheless, due to their highly porous morphology, low load bearing capabilities, high wear rates and very poor ambient environment stability, the pure TMDs did not meet the long-term industrial sliding/tribological applications [1–7]. Metal [8–24] and non-metal [1,25–32] alloying were studied to rescue these issues. However, the non-metal alloying (e.g. C or N) is preferred over metal alloying due to some drawbacks of the latter. Metal alloying is not favourable (especially in industries) due to: (i) higher operating costs of some metals, e.g. Au; (ii) not significant and short lived tribological performance achieved in comparison to the pure TMD coatings; (iii) potential selective oxidation of metals like Ti that can result in an adversely negative impact for the industrial applicability. In fact, oxidation causes generation of abrasive particles at the sliding interface which can result in high wear and, in some cases, coating failures; (iv) formation of the easy shear tribolayer can be hindered if hard metal particles remain in the contact zone/wear track and (v) the recommended alloying contents of metals (e.g., for Ti, Cr), are low that results in non-compact, sometimes quite porous and columnar morphology, thus reducing the load bearing and moisture resistance capabilities of these coatings.

Non-metal alloying got major attention as it did not display the aforementioned metal alloying issues. Overall, for alloyed-TMD coatings, the low hardness and porous morphology were resolved to a significant extent. On contrary, the efficient tribological properties in diverse environments was still an issue to be addressed. Additionally, systematic research on alloyed-TMDs is also missing in previous literature. Considering these limitations reported in the literature, our group took the responsibility to systematically study C-alloyed transition metal dichalcogenide (TMD-C) coatings during recent years [28–31,33–35]. The research evolved from lab-scale to semi-industrial scale optimization.

However, some industries use only a single target (i.e., TMD) sputtering approach, due to the requirements of cost cutting and ease of the deposition process. Thus, reactive sputtering for alloyed-TMDs appears to be the key preference over co-sputtering set ups. In such cases, C-alloying becomes unsuitable as it needs carrier gases like C_2H_2 or CH_4 . This is due to the fact that the use of carrier gases reduces the sputtering efficiency and, on the other hand, causes complexities with impurity incorporation (e.g. hydrogen) in the coating matrix. Likewise, H_2S formation cannot be avoided which adversely affects the stoichiometry and, in-turn, deteriorates the easy shear properties of the system [33,36–43]. The best green solution for avoiding these problems is the use of an environmentally neutral gas. Hence, N-alloying is the best available option for industries preferring reactive sputtering systems. Besides the purity, N-alloying additionally offers an important benefit during tribo-sliding over the deposition with C, N can evaporate as N_2 gas [44]. Hence, preventing any adverse effects (like abrasive wear inside the wear track or the

generation of wear debris near the contact zones) on the sliding performance of the components. These additional benefits potentially add up to the synergistic of easy shear TMD tribolayer formation and long-term stability of the machines/components.

Despite all the benefits, N-alloyed transition metal dichalcogenide (TMD-N) coatings have not been explored enough in comparison with TMD-C system and needs further investigation. Most importantly, the development of a stable TMD-N coating system requires a proper optimization and investigation. In the past literature, the major focus was towards the investigation of N-alloyed WS_2 (or W–S–N) coatings [37,41,42,45–51]. Despite this significant research on W–S–N coatings, still an organized study is missing. For instance, the room temperature tribological performance of WS_2 is reported in almost all literature, but testing in dry N_2 has only been superficially explored [42,48,52]. At the same time, up to our knowledge, there are no reports of the sliding performance of W–S–N coatings in vacuum while, only one study reports the high temperature tribological studies (under 3 N applied load) of these coatings [51]. The main point which we want to convey is that: for the development, optimization or at least detailed exploration of W–S–N coatings for diverse environment sliding applications, a systematic study in different environments is needed. This should be done by testing one set of coatings in different environments, so that a proper property–performance relationship is shared with the scientific community. Similarly, another important point is that most of the room temperature tests performed in ambient air, vacuum and dry N_2 published in the literature on the TMD-N coatings reports the testing performed at or below 5 N [42,45,48,52–54]. There are only few studies (ref [26,37,41,47]) that report the ambient air room temperature tribological testing of TMD-N coatings at 10 N applied loads while, no reports are present for tests performed under 10 N in any other atmosphere. Contrarily, for TMD-C coatings, 10 N is, at least, a load which almost all studies have reported. So, considering this last point, comparison between TMD-C and TMD-N coatings will be more viable if the sliding performances under 10 N applied load can be explored for various environments. Lastly, based on our recent experience with TMD-C coatings [30,31], it seems possible to optimize the crystal structure of TMD-N coating in such a way that it can be preferentially oriented in (002) direction for efficient lubrication. This optimization of deposition approach to achieve these structural properties is also needed, as it significantly enhances the sliding properties.

Considering the above-mentioned research gaps and issues, this work is dedicated to the optimization of TMD-N coatings for industrial applications. Mainly, the presented research deals with the optimization of DC sputtered W–S–N coatings with respect to morphology, crystal structure and mechanical properties. This is followed by a systematic exploration of the tribological properties of W–S–N coatings at room temperature in ambient air, at 200 °C and in dry N_2 , while, sliding under an initial contact pressure of ~1 GPa. In the end, a very brief comparison is also discussed between W–S–N coatings developed in this work and the recently reported W–S–C coatings studied by our group.

2. Experimental procedure

The reactive direct current magnetron sputtering (DCMS) of pure WS₂ and a series of N-alloyed WS₂ coatings were carried out in a Hartec® deposition chamber. The original chamber provided by the company was equipped with only one cathode but was later modified using inhouse facilities to accommodate an extra cathode. The top view schema of the deposition unit is shown in Fig. 1.

The cathode 1 was assigned to WS₂ target (99.9% purity) and the cathode 2 was assigned to a Cr target (99.99% purity) which was used for the deposition of interlayer and gradient layers. Both targets 140 cm × 140 cm × 0.8 cm in dimensions. In this research work, two different types of substrate materials were used-a) polished AISI 52100 steel (Ø 25 × 7 mm) and polished Si (111) substrates for adhesion critical load, tribology, chemical composition, deposition rates, coating thickness, cross-section and surface morphology, crystal structure and mechanical properties analysis. For the preparation of the steel substrates, they were first grounded in steps using emery papers (grit sizes = P180 to P1200) and then fine polished using diamond suspension (size = 3 µm) to achieve a final roughness (Ra) less than ~0.05 µm. For the chamber preparation, the chamber wall coverings were removed and cleaned using sand blasting to avoid contaminations from previous use. This was followed by chamber assembly, target placement and target discharge. Next step was substrates placement in the chamber, prior to which, they were ultrasonicated in acetone and ethanol for 15 min each. Substrates were dried with hot air and attached to the sample holder (rotation speed = 10 rev/min) located at a substrate to target distance of 10 cm. The chamber was then pumped down to a base pressure of 1×10^{-5} Pa. Prior to each deposition, both targets and substrates were sputter cleaned in Ar gas atmosphere under 0.3 Pa pressure. This cleaning was carried out in a systematic way: in the first phase, Cr target was cleaned for

20 min by applying a DC power of 500 W, with shutter in front to avoid cross-contamination. Simultaneously, the etching of substrates was carried out by applying a pulse negative voltage bias of 240 V, frequency of 250 kHz and pulse-on time of 1600 ns. The second phase of cleaning began after 20 min, when the power applied to Cr target was turned off, the power to WS₂ (P = 350 W) was turned on and the shutter was moved in front of it. The time duration of this stage was also kept same i.e., 20 min and after which, the target cleaning and substrate etching were terminated. Before final depositions, Cr interlayer and Cr-WS₂ gradient layers were deposited for adhesion enhancement. Cr interlayer was deposited by applying a power of 1200 W to Cr target for 5 min and maintaining a pressure of 0.53 Pa. For gradient layer deposition, the pressure was changed to 0.3 Pa, the WS₂ target was switched on. For the next 5 min, the power of WS₂ target was fixed to 350 W while, the Cr target power was gradually reduced to 0 W.

For all the final coating depositions, the DC power applied to the WS₂ target was fixed to 350 W. The N gas flow rate was varied to achieve the compositional and other property variations. For pure WS₂ coating, N gas flow was 0 sccm while for W–S–N coatings, the flow rates of 5, 12.5 and 20 sccm were used. A deposition pressure of 0.3 Pa and 120 min total deposition time were used at this stage. A list of the deposited coatings and their main deposition parameters are shown in Table 1. Note that from now onwards, the coatings will be designated as mentioned in Table 1.

Chemical composition of the coatings was accessed by wavelength dispersive spectroscopy (WDS). The WDS detector is attached to the field emission scanning electron microscope (FESEM) and is operated through INCA software. The analysis was performed with 15 kV accelerating voltage.

For the observations of the surface and cross-sectional morphologies, FESEM was used. Surface morphology micrographs were acquired as it is from the as deposited coatings while, freshly cut surfaces were used for cross-sectional images. In both cases, magnification of 15 kx were used. The coatings deposition rates were calculated using the thickness measured from cross-sectional micrographs.

For the crystal structure analysis, X-ray diffraction (XRD) utilizing copper K_{α1} ($\lambda = 1.5406$ Å) and operating in grazing (3°) mode was used.

Mechanical properties namely, hardness and reduced Young's modulus were measured by nanoindentation equipment using the method developed by Oliver and Pharr [55]. A Berkovich diamond indenter was used for indenting the deposited coatings under 2 mN applied load. The applied load

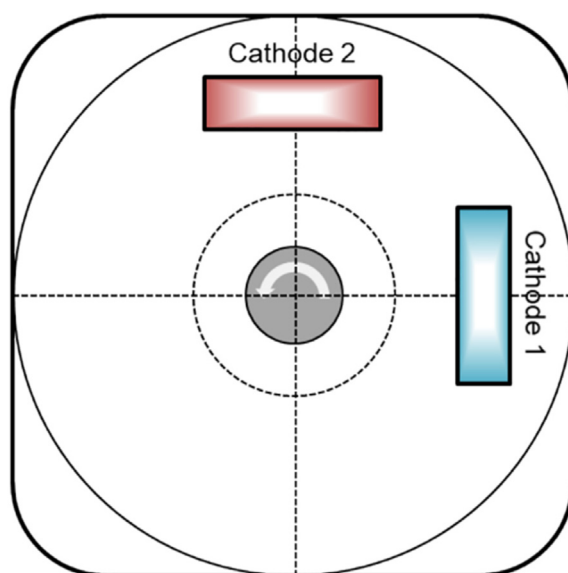


Fig. 1 – Top view schema of the deposition chamber and target arrangement.

Table 1 – Main deposition parameters used during the synthesis of the coatings.

Coatings designation	WS ₂ target power (W)	N ₂ flow (sccm)	Ar flow (sccm)	Total deposition time (min)
WS _x	350	0	21.9	130
WSN5	350	5	21.9	130
WSN12.5	350	12.5	21.9	130
WSN20	350	20	21.9	130

was selected after some preliminary tests using dissimilar loads with the aim to use a load such that the total indentation depth remains less than 10% of the final coating thickness. For each sample, measurements were taken from two different zones. A total of 16 measurements were acquired at each zone and then, the average was calculated. Measured values of hardness and reduced Young's modulus were later used for the calculations of elastic strain to failure and fracture toughness (H/E^* and H^3/E^{*2} , respectively) of the deposited coatings.

Adhesion critical loads were measured using scratch testing apparatus. A Rockwell indenter with tip radius of 0.2 mm is used to scratch the coatings under a progressive loading of 5–40 N. The conditions selected for scratching were 10 mm/min scratch speed and 100 N/min of loading rate. The substrates were then observed in optical microscope to quantify the resistance against scratch and failure mechanisms.

Finally, after all the above-mentioned characterizations, the most important testing i.e., tribological tests were carried out. Tribological tests were performed at room temperature in ambient air (relative humidity = ~35–45%), at 200 °C and in dry N₂ atmospheres using an Optimol SRV testing equipment operating under reciprocating sliding movement. A 100Cr6 steel ball of 10 mm diameter operating under 10 N applied load (initial Hertzian contact pressure = ~ 1 GPa) was used as counter body. The stroke length, linear sliding velocity and reciprocating frequency were fixed to 2 mm, 0.1 m/s and 25 Hz, respectively. The maximum total selected sliding duration was set to 1200 s, resulting in a total of 60,000 cycles (one pass is considered as one cycles). This duration was selected based on preliminary tests to ensure that the coatings do not totally worn-out. In the post tribological testing, imaging of wear scars on the wear tracks of the coatings was carried out in an optical microscope. For the calculations of the wear volume, the wear profiles were acquired using stylus profilometer (Surftest SJ-500). Wear volume, applied load and sliding distance were used to calculate the specific wear rates of the coatings, according to Archard's law [56].

3. Results

3.1. Chemical composition and deposition rates

The chemical composition, S/W ratio, coating thickness and deposition rates are presented in Table 2. During WDS analysis, the quantifications were acquired with and without oxygen and carbon, but only the latter ones are shown. Overall, the WS_x coating display the maximum contribution of these C and O contaminants when compared to W–S–N coatings.

Increasing N flow leads to a significant reduction of the contaminants.

WS_x coating is sub-stoichiometric with S/W value of ~1.5, instead of 2. Due to this low ratio, the designation for the pure coating is assumed as WS_x, and not WS₂. It will be seen later that this will have an impact on the cross-section morphology of the WS_x coating. As expected, increasing N flow rate triggers an increase in the N content of the coatings in the range of ~14–~26 at. %. With the introduction of even the lowest amount of nitrogen in the WS_x coating, S/W ratio show a significant decrease. WSN5 coating having 14.6 at. % N displays a S/W ratio of 1.17. Increasing the nitrogen content to 23 at. % for the WSN12.5 coating results in an additional decrease of the ratio to 0.99. With further increments in the N flow to 20 sccm, the ratio does not significantly change.

The measured deposition rates of the final coatings are presented in Table 2. The WS_x coating show a deposition rate of 17.3 nm/min, which is the lowest among all the deposited coatings. With the introduction of N in the chamber, the deposition rate increase to 20.3 nm/min for the WSN5 coating and it is actually the maximum deposition rate measured. With further increase of the N flow rates to 12.5 sccm (WSN12.5) and 20 sccm (WSN20), the deposition rates decrease to 18.1 nm/min and 17.7 nm/min, respectively.

3.2. Surface and cross-sectional morphology

The surface and cross-sectional morphologies of the coatings are shown in Fig. 2. Three zones can be distinguished in the reference WS_x coating: interlayer, gradient layer and final coating. The WS_x coating is slightly porous as compared to the other coatings. This WS_x coating displays a columnar cross-sectional morphology with spaces between the columns. Similarly, the porosity is also visible in the surface morphology micrographs. Despite this porosity, the grains grew in a cauliflower type morphology (caused by limited surface mobility). This morphology contradicts the morphologies of most sputtered pure TMD coatings reported in the literature, where needle/sponge like morphology has been reported [1,32,34,57].

With the introduction of N in the chamber, the coatings become compact. The coating with lowest N (WSN5 coating) displays a dense columnar cross-section morphology and a cauliflower surface morphology (like WS_x coating). However, this coating seems to be more compact than the WS_x coating. This means that the porosity is reduced to a greater extent. With further increments in the N content, compactness continues to increase with no vestiges of the columnar morphology or porosity evident from cross-sectional micrographs. The WSN20 coating with the highest N is the most compact and nearly featureless one. In all the N-alloyed

Table 2 – Chemical composition, S/W ratio, thickness and deposition rates of coatings.

Coatings	N (at. %)	W (at. %)	S (at. %)	S/W	Final coating thickness (μm)	Deposition rate (nm/min)
WS _x	—	40.0 ± 1.5	59.0 ± 1.2	1.47	1.12	17.3
WSN5	14.6 ± 0.5	39.0 ± 0.1	45.6 ± 0.5	1.17	1.21	20.3
WSN12.5	23.0 ± 1.8	38.1 ± 0.9	37.9 ± 0.8	0.99	1.16	18.1
WSN20	25.5 ± 0.2	35.6 ± 0.4	38.1 ± 0.2	1.07	1.10	17.7

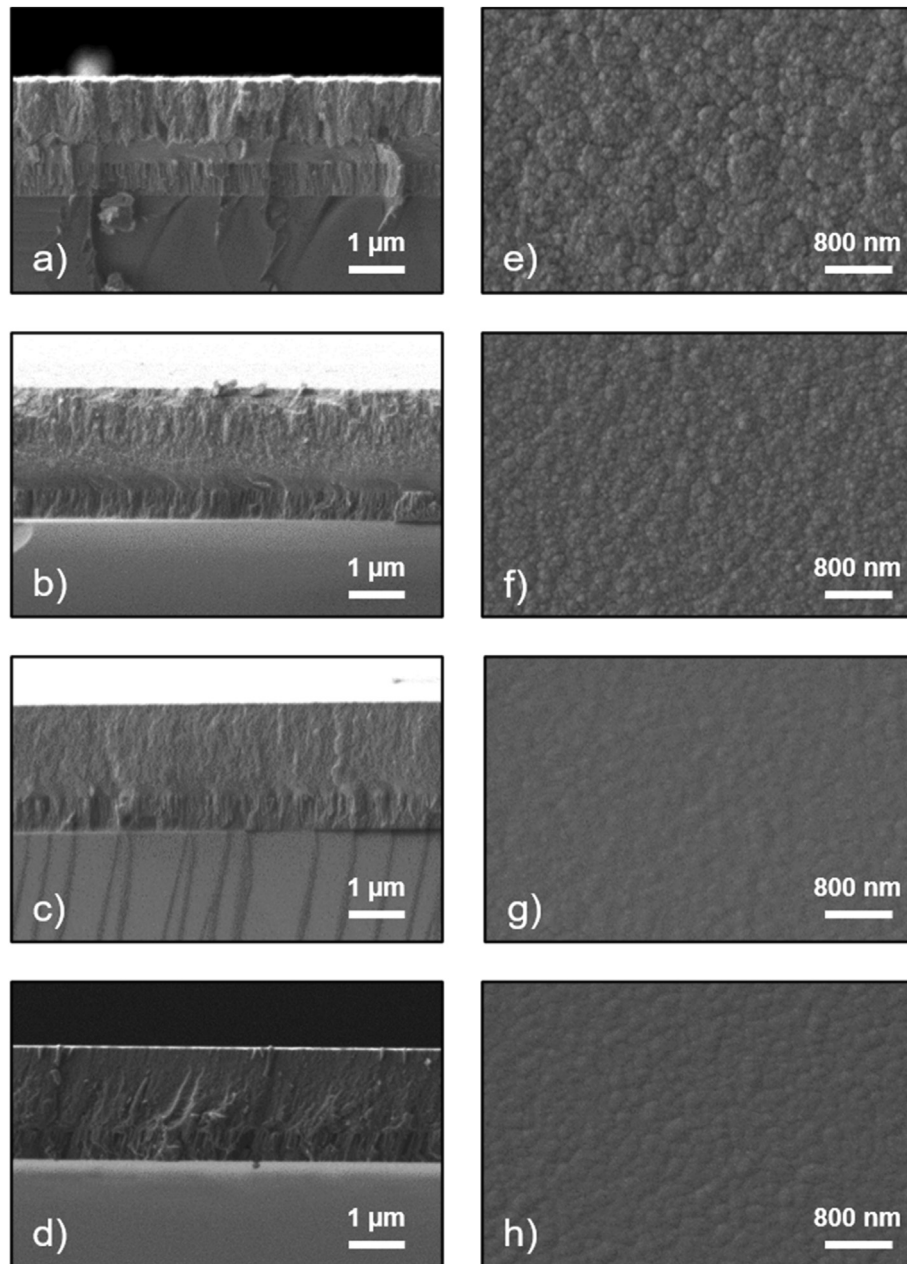


Fig. 2 – Cross-section and surface morphologies of the coatings – cross-section morphology: a) WS_x, b) WSN5, c) WSN12.5, d) WSN20 and surface morphology: e) WS_x, f) WSN5, g) WSN12.5, h) WSN20.

coatings, it is hard to distinguish the gradient layer due to their similarity to the top coating's morphology. Regarding the surface morphologies of WSN12.5 and WSN20, the micrographs depict very smooth surfaces with only minor features visible and no porosity.

3.3. Structure

X-ray diffraction patterns of the deposited coatings are displayed in Fig. 3. The WS_x coating displays a X-ray pattern typical of sputtered TMD coatings. The (100) peak observed at ~33 - 45 is broad and displays an extended shoulder, which is a typical feature of sputtered TMDs. Wiese et al. [58] explained

that this broadness of peak happens due to the turbostrating stacking of the 10 L planes ($L = 1, 2, 3, \dots$). Some minor peaks related to both pure WS₂ and substrate are also observed at ~62 and ~71. Two very crucial observations that should not be ignored here are: i) the shift of the diffraction peaks to the left, when compared to the pure WS₂ standard (ICCD card: 087–2417) and ii) the broadness of the diffraction peaks. For example, the centre of (002) shifts from standard 14.3 to ~12 and moreover, it is quite broad. This will be further explained in the discussion section.

With N additions, for both WSN5 and WSN12.5 coatings, the preferential orientations shift from (100) to (002), and the intensity of the (002) peak increases. The centre point of the

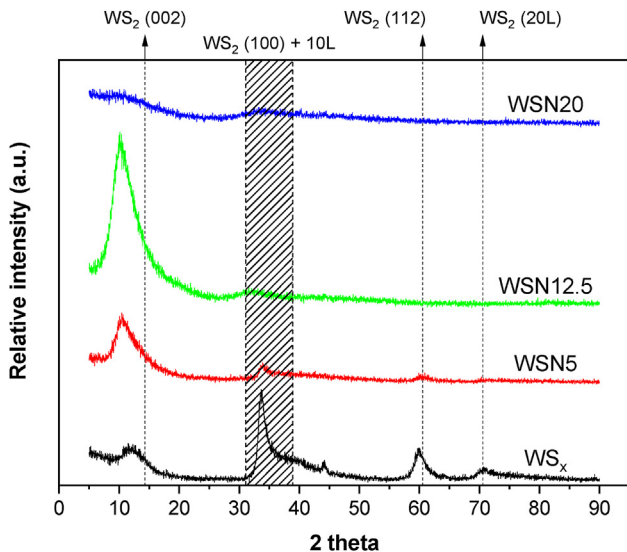


Fig. 3 – XRD diffractograms of the coatings acquired in the grazing incidence mode.

(002) diffraction peak shifts more towards lower angles and the peak broadness increases. The presence of the (002) peaks and peak shift to lower angles are expected to positively affect the tribological properties of these coatings as reported in ref [30]. Finally, for WSN20 coating, the structure is broad with no well-defined peaks. This means that addition of third element above a certain value disturbs the structural growth of TMD crystals and make them XRD amorphous [31,32,52]. Actually, very small WS_2 nanocrystals might be present in this coating, but as XRD has a limitation that it cannot detect particles less than ~5 nm, the obtained pattern is quite amorphous [31].

3.4. Mechanical properties

The mechanical properties of coatings play a vital role in the long-term durability and load bearing characteristics of the coatings. For the analysis of mechanical properties, adhesion critical load, hardness, elastic strain to failure and fracture toughness measurements were performed. The results of these analysis are shown in Table 3. All the coatings display the first onset of the adhesion failure, Lc2 only. In quantitative terms, the WS_x coating displays Lc2 value of 9.5 N which increases to 18 N for the coating with lowest N content (WSN5). This Lc2 becomes 20 N and 21 N for WSN12.5 and WSN20, respectively. So, increasing N increases the adhesion critical loads of the coatings. Overall, the coatings are strong enough to resist delamination from the substrates and even for the WS_x coating, no Lc3 failure is detected. From our previous experience [34], the adhesion of the coatings shows satisfactory results with expectations of good tribological results.

The hardness of the WS_x coating is ~3.7 GPa which is higher than the values reported in literature for pure TMD coatings, where coatings display hardness less than ~1 GPa [34,37,54,59,60]. While comparing all W-S-N coatings, the hardness increases from ~6.6 GPa (WSN5) to ~8.0 GPa (WSN12.5) and then decreases to ~7.2 GPa (WSN20 coating). Also, the Young's modulus values increase with increasing N content.

Table 3 – Ahesion critical loads, hardness, reduced Young's modulus, elastic strain to failure and fracture toughness of the deposited coatings.

Coatings	Lc2-Adhesion critical load (N)	Hardness (GPa)	E*-Reduced Young Modulus (GPa)	H/E*	H^3/E^{*2}
WS_x	9.5 ± 0.2	3.7 ± 0.5	69.5 ± 2.3	0.05	0.01
WSN5	18.0 ± 0.4	6.6 ± 0.3	73.5 ± 1.7	0.09	0.05
WSN12.5	20.0 ± 0.2	8.0 ± 0.2	82.8 ± 2.6	0.10	0.07
WSN20	21.0 ± 0.6	7.2 ± 0.3	96.0 ± 3.1	0.08	0.04

Finally, in this section, the parameters related to elastic strain to failure (H/E^*) [61], and fracture toughness (H^3/E^{*2}) [62], are calculated as presented in Table 3. These values are related to the elastic energy storage in the materials and to the wear resistance of the materials, respectively. Higher values of these parameters are considered better for the tribological performance [63]. In present study, these values follow same trend as hardness, so, it is expected that the WSN12.5 coating will out-perform the rest.

3.5. Tribological performance

The tribological tests were performed for all the coatings to analyse the combined effects of all above mentioned properties on the sliding performance in ambient air at room temperature, at 200 °C in ambient air and in dry nitrogen atmospheres.

3.5.1. Coefficient of friction and specific wear rate at room temperature

Figure 4 shows the average friction co-efficient (COF) and the specific wear rate values of all the coatings at room temperature in ambient air. The average COF values are calculated from the steady state regions of the friction curves. In all the coatings, the starting point for average calculation is fixed at 200 s. This is because the coatings are efficiently sliding in the steady state zone. The end point is either the end of the testing durations (for coatings sustaining the whole test) or a point just before a sharp spike in the COF is observed (for the coatings that could not sustain the whole testing duration). Similarly, for the wear rate calculations, the tracks are studied from the tests that were stopped just at the very beginning of the spikes in COF. The idea behind this approach is to study wear while remaining inside the final coating and not in the gradient/interlayer.

The average steady state COF of the WS_x coating is 0.09. This coating starts to worn out after 820 s, which results in a sharp increase in the COF. However, it shows a high specific wear rate value of $4.1 \times 10^{-7} \text{ mm}^3/\text{Nm}$. The WSN5 coating displays the highest average steady state COF of 0.15. Irrespective of the increments in the COF, the specific wear rate is quite low as compared to the WS_x coating i.e., $1.0 \times 10^{-7} \text{ mm}^3/\text{Nm}$. Also, the WSN5 coating sustains the whole sliding duration without any signs of wearing through the gradient layer. As the N is further increased (WSN12.5), the COF again decreases to 0.09, with coating sustaining the whole test duration. This coating displays the most stable COF response. The

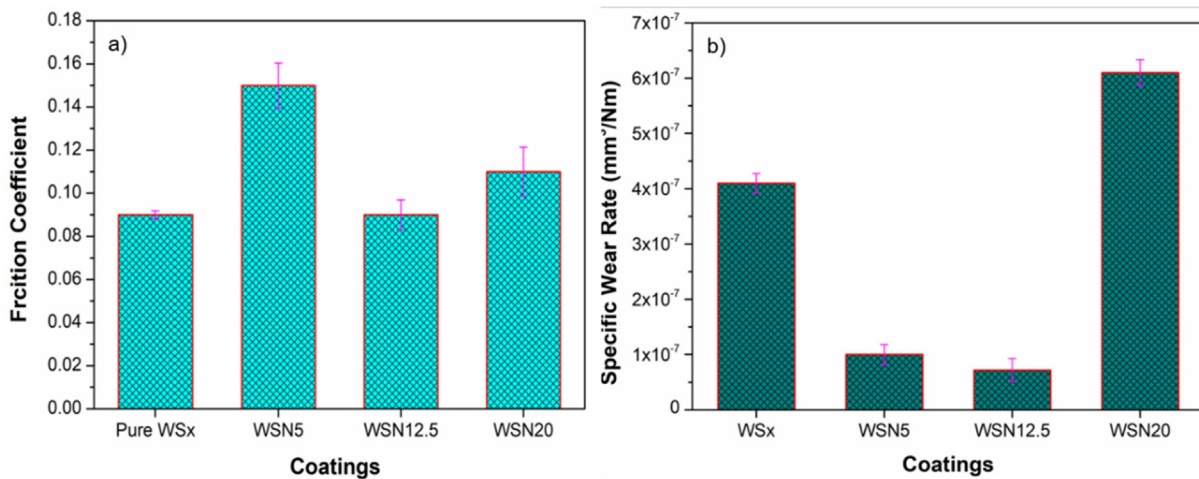


Fig. 4 – Average steady state friction coefficient (a) and specific wear rates (b) of coatings tested at room temperature in ambient air.

specific wear rate of 7.2×10^{-8} mm³/Nm, for this coating is also the least observed among all deposited coatings. Finally, the coating with highest N content (WSN20) displays an average COF value of 0.11, with the maximum sliding limit of 920 s. The frictional response of this coating is very poor, highly unstable even in the steady state region. Furthermore, it displays the highest specific wear rate of 6.1×10^{-7} mm³/Nm among all the coatings. Overall, the specific wear rates of pure and WSN20 coatings are very close to each other.

3.5.1.1. Wear track images. For all coatings, the selected wear track images are presented in Fig. 5, while their corresponding cross-sectional wear profiles are shown in figure S1 of the

supplementary document. Two different morphological zones are evident from the wear track image of the WS_x coating. The track is partially covered with the tribolayers, as marked by points T. Rest of the zones have similar morphology as point C and are not covered by the tribolayer. The maximum depth of the wear scar detected by the profilometer is ~0.9 micron. This means that although the gradient layer is not exposed, the sliding was occurring at the near verge of outer/final coating removal. This agrees with the fact that the testing was halted just at the very beginning of the spike in the COF. WSN5 coating's wear track is covered with the tribolayer zones in the middle areas only. Tribolayer is not detected on the side regions. Both these zones/morphologies are marked by letters T

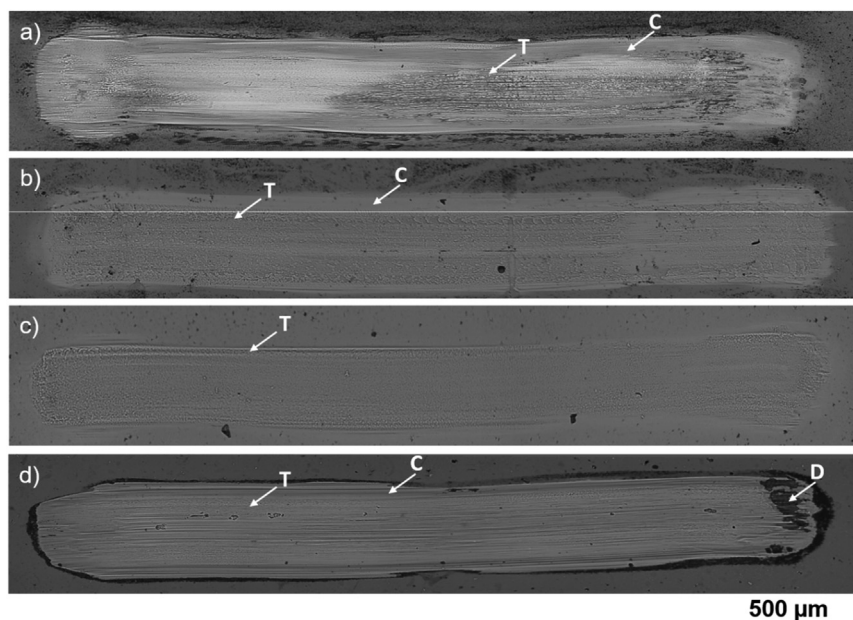


Fig. 5 – Typical wear track of the: a) WS_x, b) WSN5, c) WSN12.5 and d) WSN20 coatings tested in ambient air at room temperature.

(tribolayer) and C (uncovered). The maximum wear scar depth detected by the profilometer is ~0.37 microns, proving the sliding is occurring inside the final coating. The wear track of the best performing coating, WSN12.5, is fully covered with the tribolayer. No morphological differences are evident from the wear track images. This means that during testing, the sliding was always governed by the tribolayer. This sliding mechanism coupled with the wear track uniformity is the key reason behind the highly stable and efficient frictional performance of WSN12.5. The maximum wear scar depth is merely 0.25 microns, justifying its superior wear resistance than other coatings. For the coating with the highest N concentration i.e., WSN20, although the average COF is not much different from WSN12.5, the instability in frictional response and early failure are related to the fact that most of the wear scar is not covered by the tribolayer and at the same time, excessive abrasive wear is detected as marked by point D (the reasons are discussed thoroughly in section 4.2). The tribolayer and uncovered zones are again marked by same points T and C, respectively. Further, the wear scar profiles clearly show that the sliding was mostly occurring against the gradient layer as the maximum measured depth is ~1.25 microns (against 1.1 micron of outer coating thickness). The Raman spectroscopy was used to identify the different zones. The Raman spectra from tribolayer and as-deposited coating zones for one of the coatings is shown in supplementary material, as a reference.

3.5.2. Coefficient of friction and specific wear rate at 200 °C
The achieved average COF and specific wear rates of the coatings tested at 200 °C in ambient air are shown in Fig. 6. Similar to the tests performed at room temperature, the average COF values are calculated from the steady state region. Unlike the room temperature tests, the starting points of the steady state calculations are not fixed to 200 s, as each coating displayed its own specific steady state beginning time. For the selection of the end point of the steady state zone and the specific wear rate calculations, similar procedure is followed as has been reported for the ambient air testing.

In the present case, the WS_x coating displays an average COF value of 0.04 which is much less than the room temperature average COF. The steady state zone of this coating starts

from 150 s and lasts till 850 s, after which, continuous spikes in the COF are observed. The specific wear rate just before the start of spike zone is 3.0×10^{-7} mm³/Nm, a value highest among all the 200 °C tests. The WSN5 coating's steady state zone starts from 350 s and lasts till the end of the testing duration. The average COF displayed by this coating is 0.05. Although the COF of WSN5 also decreases from room temperature to high temperature tests, this value is still higher than all other coatings. This means that similar trends to room temperature testing are observed when the coatings are compared to each other. A specific wear rate of 1.3×10^{-7} mm³/Nm is shown by this coating. With increasing nitrogen, similar to the room temperature tests, the WSN12.5 coating displays the best sliding properties with respect to both the COF and specific wear rate. The average COF value of 0.02 is shown by this coating in the steady state zone which starts from 400 s and lasts till the end of the test. The specific wear rate of 7.1×10^{-8} mm³/Nm is shown this coating. Finally, despite the environmental shift, the highest N-alloyed WSN20 coating again displays unstable friction. It is not possible to differentiate/select a steady state zone. The COF remains fluctuating throughout the test. It gradually increases till 800 s and then gradually decreases till the end of the test. Opposed to what is observed in the room temperature sliding, at 200 °C, the coating sustains the whole testing duration. An average COF of 0.02 and specific wear rate of 1.6×10^{-7} mm³/Nm are observed.

3.5.2.1. Wear track images. Figure 7 shows the wear track images of the tested coatings at 200 °C. Similar to the tracks of room temperature testing, the tracks of WS_x coating after 200 °C show different morphological zones i.e., the tribolayer and the as-deposited coating like areas. This non-homogeneity and less tribolayer coverage of the wear track is the reason why the COF increased after a certain number of the sliding cycles. This is also in agreement with the wear track profiles, shown in figure S2 of the supplementary document. The maximum depth observed is close to 1 micron, a value almost closer to the exposure of the underlayers. This relates well with the increase in the COF after certain sliding cycles. It should be mentioned again that the shown track is related to the test which was stopped just at the beginning of

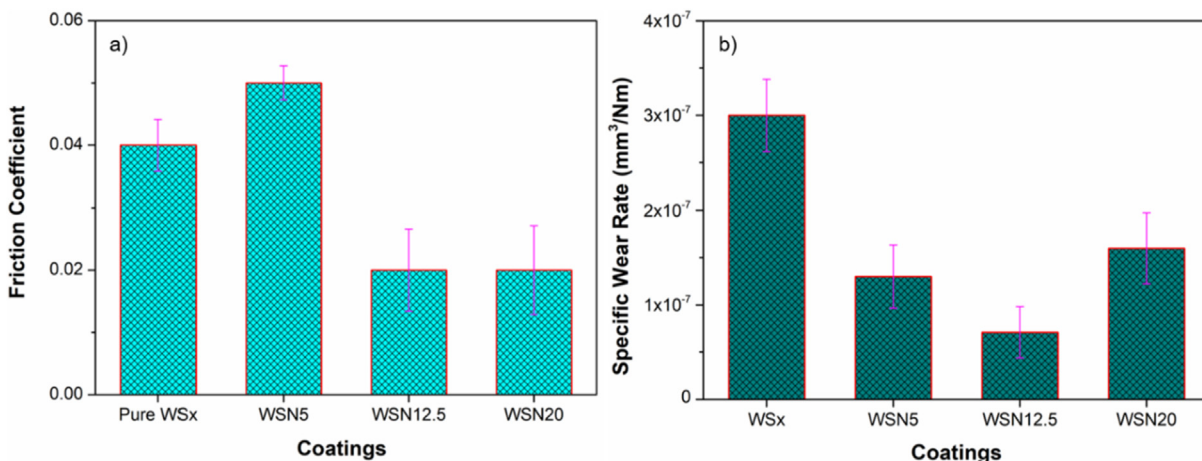


Fig. 6 – Average steady state friction coefficient (a) and specific wear rates (b) of coatings tested at 200 °C in ambient air.

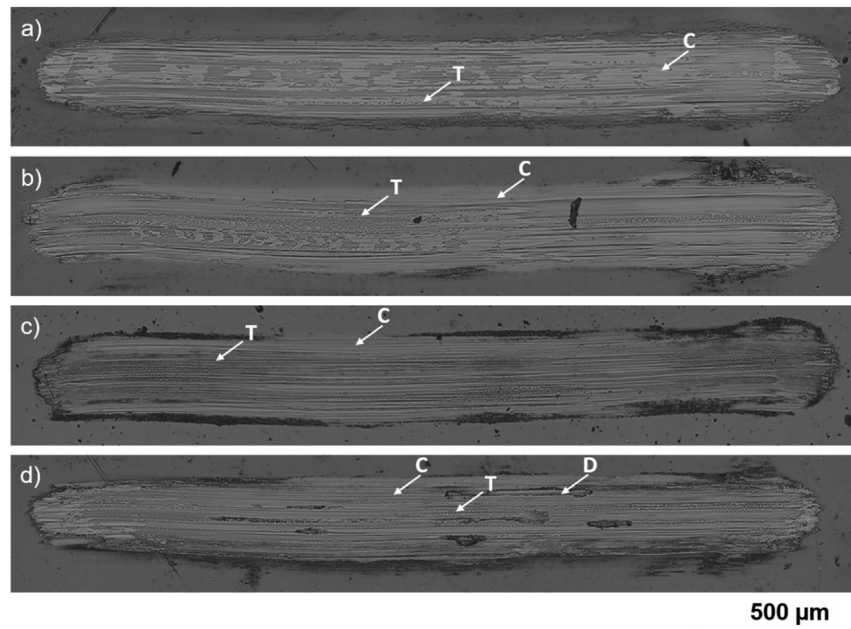


Fig. 7 – Typical wear track of the: a) WS_x, a) WSN₅, c) WSN_{12.5} and d) WSN₂₀ coatings tested at 200 °C in ambient air.

the friction spike. For WSN₅, almost similar tribolayer zones are observed as in the WS_x coating. The higher load bearing capability of this coating results in a maximum observable wear depth of 0.8 micron, a value slightly lower than the WS_x. Despite the fact that the difference in wear track depth is not very pronounced, the high wear resistance or better mechanical properties help this coating to sustain sliding throughout the testing duration. As in the room temperature test, the WSN_{12.5} coating displays superior high temperature friction and wear properties, probably due to a more homogeneous wear track morphology. Although, abrasive wear marks are observed, the homogeneity coupled with high hardness helps to sustain the load much better than others. A maximum wear scar depth of solely 0.5 micron is detected, a value half than the highest value observed in this testing condition. This wear depth analysis observation corroborates well with the above-mentioned specific wear rate of this coating. The WSN₂₀ coating wear track is again the worse among all with clear signs of some worn through zones (marked by D). The presence of the highest N results in a high amount of hard particles which cause aggressive wear at some points. The maximum wear track depth, except the worn through zones, is 1.0 μm . This means that when the test was stopped, the coating was at the verge of failure. Although, the coating lasts the whole test duration, the wear track and wear depth further unveil the reasons of unstable COF behaviour.

To summarize, after moving from room temperature to 200 °C, generally the COF and specific wear rates are decreased.

3.5.3. Coefficient of friction and specific wear rate in dry nitrogen

The COF and specific wear rates of all coatings after sliding in dry N₂ are shown in Fig. 8. All the coatings bear whole

sliding duration, unlike the tests in other atmospheres. The WS_x coating displays a steady state average COF value of 0.02 and a specific wear rate of $5.0 \times 10^{-8} \text{ mm}^3/\text{Nm}$, both lower than what is observed in the other sliding atmospheres. The COF reaches a value of 0.03 after only 13 s, but continues to decrease till 600 s, after which the steady state is reached. For WSN₅ coating, the average steady state COF and specific wear rates are 0.03 and $9.3 \times 10^{-9} \text{ mm}^3/\text{Nm}$, respectively. The steady state starts almost after 50 s of sliding duration. Contrasting the sliding behaviour observed at room temperature and at 200 °C, this coating behaves exceptionally well here. For the first time, this coating displays such a lower COF and the least wear rate than any other coating. The WSN_{12.5} coating frictional behaviour is similar to the WSN₅ coating i.e., it displays an average steady state COF of 0.03 and this steady state zone starts right after 45 s of sliding. The specific wear rate is $1.2 \times 10^{-8} \text{ mm}^3/\text{Nm}$, which is again very close to the WSN₅ coating and the minor difference can easily be neglected. Lastly, the WSN₂₀ coating steady state begins after 350 s and surprisingly, the frictional behaviour is very stable. An average steady state COF of 0.04 and specific wear rate of $2.2 \times 10^{-8} \text{ mm}^3/\text{Nm}$ are displayed by this coating. Despite the difference in the values is very small, this coating displays the highest COF among all coatings and highest wear among the N-alloyed coatings.

3.5.3.1. Wear track images and profiles. The wear track images of the tests in dry N₂ are shown in Fig. 9, while the corresponding cross-sectional wear track profiles are shown in figure S3 of the supplementary material. All the wear tracks are quite smooth and homogeneous, different from the observations in other atmospheres, where a lot of morphological differences were observed. This homogeneity of the wear tracks can be related to: 1) the highly stable

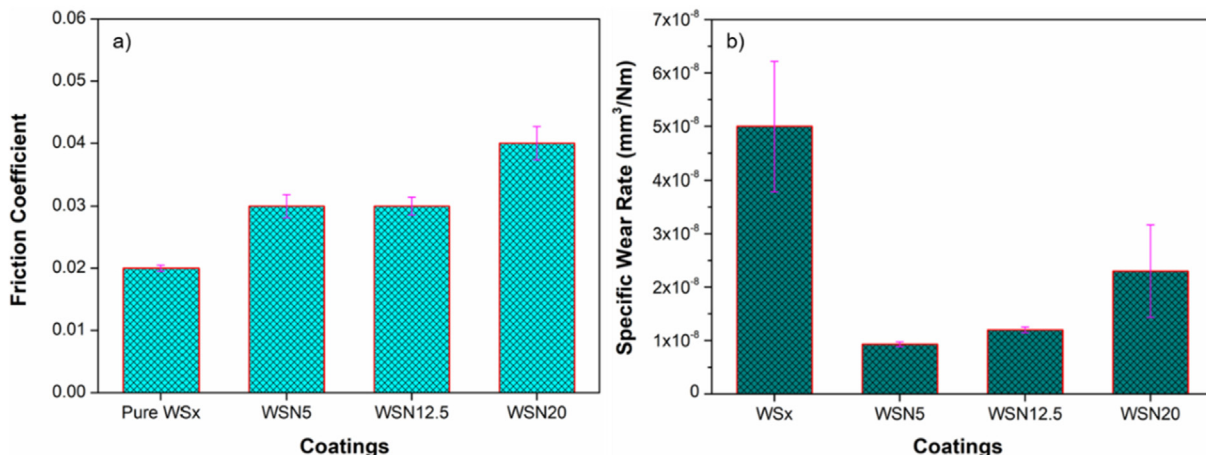


Fig. 8 – Average steady state friction coefficient (a) and specific wear rates (b) of coatings tested in dry nitrogen.

and steady frictional behaviour and 2) the efficient sliding performance to complete the whole sliding duration than in other atmospheres. The WS_x coating wear track displays fewer abrasive marks than the other coatings which is directly linked to the N content. Therefore, the coating with the highest nitrogen displays more abrasive marks. The maximum wear scar depths measured by profilometer clearly show that the WS_x coating is worn the most followed by WSN20, WSN12.5 and WSN5, respectively. These results are in accordance with the specific wear rate observations. All coatings are efficiently sliding in the final/top coating, justifying no friction spikes or underlayers exposure are observed. To summarize, it is clear on comparison with the profiles of other environments that the coatings are much less affected by sliding in the dry N₂ atmosphere.

4. Discussion of the results

4.1. On general properties of the coatings

In regards to the composition, the sub-stoichiometry (low S/W ratio than 2) observed for the WS_x coating can be explained by: 1) the process at the substrate surface where re-sputtering of the growing coating occurs. Although, all coatings were deposited without substrate bias, there is always a minor self-bias present on the substrates which result in the attraction of Ar⁺ ions. These ions cause the potential re-sputtering process of the lighter S atoms from the growing coatings. Furthermore, during sputtering, the voltage developed at the target surface results in the generation of energetic Ar neutrals. These Ar neutrals can be reflected from the target surface and

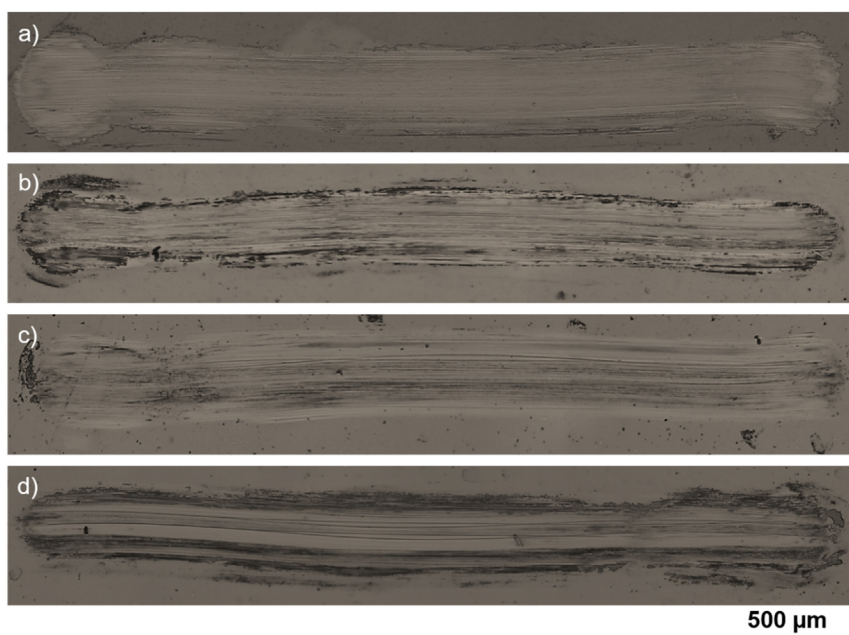


Fig. 9 – Typical wear track of the: a) WS_x, b) WSN5, c) WSN12.5 and d) WSN20 coatings tested in dry nitrogen.

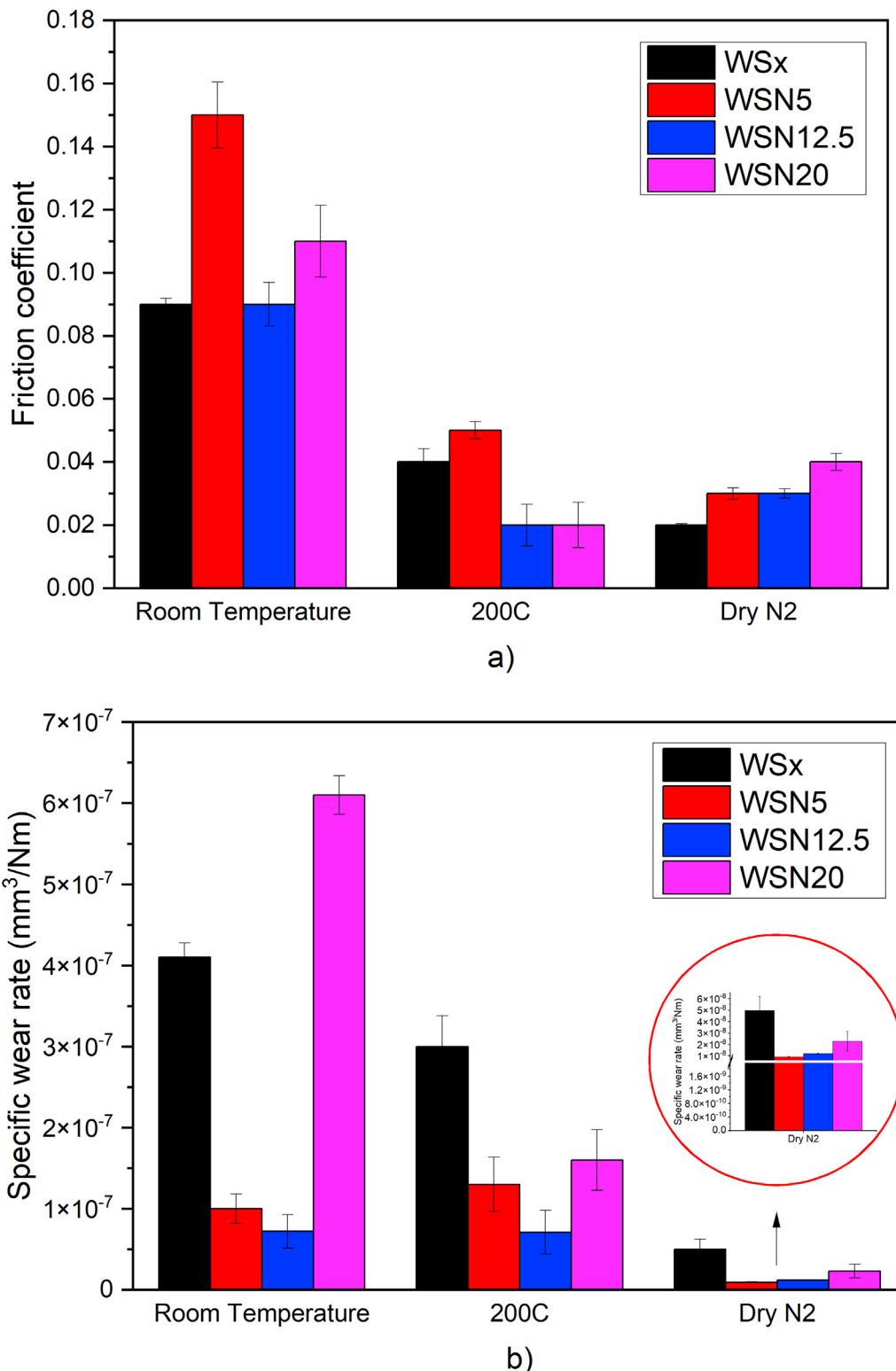


Fig. 10 – a) friction coefficient and b) specific wear rate of the coatings tested at different atmosphere/temperature conditions.

hit the growing coating with high energy and cause re-sputtering of the lighter element [28,64]. 2) the process occurring in the interelectrode space between the target and the substrate (inside plasma). As S is much lighter than W, it is more affected by the collisions with the plasma particles,

which may scatter in the chamber instead of traveling straight to the substrates. On the other hand, W is less affected by such collisions, having a higher probability to reach the growing coating. This difference in the scattering of S and W further adds to the sub-stoichiometry of the coatings resulting in

lower S/W ratio as observed in most of the studies on TMD coatings. Regarding the N-alloyed coatings, the N content does not increase linearly despite the flow rate was increased in a systematic and linear way during depositions of different coatings. This can be explained by the amount of free space or sites available inside the WS_x coating.

The increment of the deposition rates from the WS_x to the WSN5 coating is due to the fact that an additional element is introduced in the chamber. This means the sputtered elements inside the plasma increased, making the coating and the deposition rate to increase. On the other hand, the decrements in deposition rates with further increase of N flow are governed by two factors: 1) the poisoning effect of sputtering target induced during reactive sputtering. This poisoning effect is enhanced with increments in the N flow rates thus, reduces the sputtering yield of the target [65]. 2) the N additions make the coatings more compact, which decreases the deposition rate, as reported in the literature [32,34,66].

The WS_x coating morphology is different from the one of sputtered pure TMDs in most of the literature. Typically, the morphology of WS_x coatings is sponge-like with very high porosity, unlike the one observed in this work [1,26,67]. The reason for this is associated to the low S/W ratio. Anyway, this achieved morphology of the WS_x coating is a plus point, as such minorly compact coatings are capable of resisting catastrophic failures [31] and thus, can sustain for short duration sliding cycles, which is good for applications requiring one time use of the coated component. With N-alloying, the observed morphologies are in accordance with literature and as expected from our previous experiences [1,31,34], the type of morphologies observed for coatings deposited here are expected to display excellent tribological performances, as shown in section 3.5. It is reported in literature that the sputtered TMD coatings can show two types of preferential orientations, i.e., either the (100) or (002) [31,68]. In the present case, the WS_x coating displays (100) preferential orientation. Indeed, the obtained relative intensities for the (100) and (002) diffraction peaks divided by their relative intensities in the powder ICDD card of WS₂ (ICCD card: 087–2417) indicate a (100) preferred orientation. Basically, the (100) orientation dominates if the (100) planes grow nearly parallel to the surface, whilst a (002) preferential orientation dominates if the (002) planes grow nearly parallel to the surface. The WS_x coating peak broadness and shift to lower angles is related to the low S/W ratio as compared to the pure WS₂ standard. This low ratio induces structural disorders inside the coatings and thus, a shift to lower diffraction angles and peak broadness are observed. The shift of preferential orientation, from (100) to (002), increase of (002) diffraction peak intensity, their broadening and shift to lower diffraction angles with N-alloying is due to multiple factors: 1) the incorporation of N flux in the chamber. It is well understood that the re-sputtering of S causes the availability of free W, which can react with N. Such phases partially superimpose the peak of WS₂, leading to the broadening of the (002). 2) similar to the reference WS_x coating, the lower S/W ratio also shifts the XRD diffraction peaks to lower angles. This shift is enhanced with N-alloying as N can go and settle between the basal planes, causing the lattice parameter to expand (which is in agreement with the literature reports [69,70]. Additionally, N can be forming a solid solution in the TMD structure,

establishing bonds with W, resulting in a shift of the XRD diffraction peaks. This has never been reported in the literature. Thus, a detailed investigation on this hypothesis needs to be carried out. 3) the increased deposition rate enhances the deposition of second layer of (002) prior to the desorption of the first layer thus, enhances the (002) peak intensity or preferential orientation [68]. Regarding the (100) peaks, they become broader and display very low intensity, as it is not the preferred orientation after N additions. The amorphous nature of the coating with highest N concentration is not a new observation. The literature shows multiple reports where with increasing alloying contents, the structural integrity of TMDs is disturbed to the limit where the TMD crystals become undetectable in XRD analysis [31,52].

The critical adhesion load results align with the morphologies of the coatings i.e., the adhesion load increases with increasing compactness. Thus, N content is directly linked to increase of compactness and adhesion. This means that the load bearing capability increases resulting in greater crack propagation resistance.

The higher hardness of WS_x coating as compared to those reported in the literature for sputtered WS₂ coatings is related to their compact morphology (section 3.2, Fig. 1a) and consequently to the low S/W ratio. From WSx, with increasing N content, an increase in the compactness is observed. On the other hand, the incorporation of N creates more amount of phase with strong W–N bonds which further promotes an increase in hardness. For the highest content of N, the structure evolves from a nanocomposite to a complete amorphous phase which can be the reason behind the decrease in hardness value.

4.2. Tribological results

For readers convenience the COF and specific wear rates values of the coatings tested at different environments/temperatures are summarized in Fig. 10. The trends observed during room temperature tribological tests can be explained in relation to the basic characteristics of the coatings described in sections 3.1 to 3.4. Lowest COF are shown by WSx and WSN12.5 coatings. The WSx coating displays low COF due to its very soft nature. This softness leads to an easy low shear tribolayer formation of WS₂ basal planes parallel to the sliding direction. Based on our recent reports on the tribolayer formation mechanisms [71], it can be said that with softer coatings, the worn material which gets entrapped as third body is easy to align under the applied load during sliding. On the other hand, the WSN12.5 coating's efficient sliding than other N-alloyed coatings is related to the presence of (002) planes parallel to the sliding direction. This is well evident from the dominant (002) peak in XRD diffractogram (Fig. 3). Despite the (002) peaks in WSN5, it shows highest COF which can be related to the contribution from the (100) peak. This means that there are (100) planes perpendicular to sliding direction that are difficult to align during sliding, hence, contributing to the increase in the COF. WSN20 is an amorphous coating with no evidences of the (002) planes. So, the COF is higher than the WSx and WSN12.5 coatings. In case of the specific wear rates, the low compactness, softness, low hardness and low fracture toughness of WSx are the reasons behind its high specific wear rates than WSN5 and WSN12.5. The lowest specific wear

rates observed for WSN12.5 coating is due to the easy tribolayer formation (due to presence of (002) planes) coupled with highest hardness and fracture toughness. The fracture toughness resists the plastic deformation, higher hardness helps in load bearing and ultimately, when both of these are coupled with the easy tribolayer formation, the sliding occurs efficiently inside the tribolayer, preventing the wear of the coating beneath it. The WSN20 coating, on the other hand is amorphous, has hardness lower than WSN12.5, the fracture toughness is also lower than both WSN5 and WSN12.5 coatings. These are the reasons behind low wear resistance of this coating. Now, a question might arise: why a small variation is observed between the specific wear rates of the WS_x and WSN20 coatings? This can be simply explained by the different wear mechanisms taking place on the wear track of the coatings and the highly amorphous structure (no (002) orientation) of the WSN20 coating. The wear mechanism of WSN20 is more abrasive nature, leading to a high wear depth as compared to the WS_x coating. Besides, it is reported multiple times in literature that TMD coatings possess excellent ability to replenish the worn-out zones/regions [30,60,72]. So, even if some initial high wear of the WS_x coating would have happened, such zones can be replenished swiftly by the soft worn material (transferred material on ball and third body worn material) entrapped between the sliding parts. This is not so easy in the WSN20 coating as it has high nitrogen content and amorphous structure which on one hand, leads to the formation of more hard nitride particles and, on the other hand, reduces the efficient tribolayer formation. The hard particles, if stuck in the contact zone can cause abrasive wear as is the case here. Additionally, the absence/reduction of tribolayer formation means no soft material is present to cover worn out zones.

During the high temperature sliding tests of all coatings, the average values of COF and specific wear rates decrease when compared to the room temperature testing. Overall, the COF trends between the coatings are almost similar in both atmospheres. The decrease in the COF is related to the fact that temperature helps in easy reorientation and sliding of the basal planes in TMDs, and consequently decreases the resistance to sliding [73]. Although high temperature, the sliding properties of W–S–N coatings are only reported once in literature and the observations presented here are very similar to that study. If discussed individually, the WS_x coating displays slightly higher COF than the WSN12.5 and WSN20 coatings due to the fact that it is a pure coating without any alloying element, which makes it more prone to oxidation. Indeed, it is well-known that pure TMDs oxidize at lower temperatures [74,75]. An additional reason is the high porosity of the WS_x coating which allows more thermal degradation and oxidation attack. The WSN5 coating displays highest COF among all coatings due to similar reasons as explained in room temperature results. The WSN12.5 coating is again the one that displays the best COF and specific wear rate properties due to its characteristics of having a compact morphology with absence of (100) WS₂ peaks, and the presence of high intensity (002) peak. The highly amorphous WSN20 coating initial increments of the COF are solely related to the crystallization of the TMD phase under the applied load to form (002) basal planes parallel to sliding direction [66,76,77]. During this crystallization, the coating must

overcome the energy barrier resisting the atomic arrangement. It should be mentioned that the increment in COF at 200 °C is gradual with highest value of highest COF to be ~ 0.04 when compared to the friction response of the room temperature sliding where the value is much higher. This is attributed to the fact that along with the applied load and/or sliding force, an additional energy source i.e., high temperature supports the (002) crystallization and tribolayer formation process. Temperature on the one hand, can provide the energy for crystallization while, on the other hand, it also reduces the van der Waals forces of attraction. Now, while discussing the wear resistance, it can be said that the high porosity, low compactness, low hardness and low fracture toughness reduce the wear resistance of WS_x coating compared with the rest [78–80]. The lower specific wear rate of WSN5 than the WS_x and WSN20 coatings is due to the higher fracture toughness and resistance to plastic deformation. These higher values support the sliding throughout the testing duration, unlike the WS_x coating. Despite a comparatively better friction and wear performance than the room temperature tests, the wear rate of WSN20 coating is still highest among the N-alloyed coatings. This is related to the low fracture toughness than WSN5 and WSN12.5 coatings, the higher time taken for the crystallization, the absence of the steady state sliding and the partial exposure of the gradient layer (as presented in section 3.5.2.1). Overall, the best wear resistance is displayed by the WSN12.5 coating. The highest compactness, hardness, fracture toughness and plastic deformation resistance of this coating, give the highest resistance to wear.

Overall, the lower specific wear rates of coatings tested in nitrogen as compared to the ambient air and 200 °C is due to the fact that there is no moisture or high temperature oxidation affecting the sliding of the coatings [77]. Indeed, the tests were conducted at RT and the relative humidity during these tests was less than 6%. During the sliding in dry nitrogen, the COF values display an increasing trend with increasing N-alloying. Individually, the WS_x coating displays lowest steady state COF among all the coatings in dry N₂. This is directly related to the pure unalloyed nature of the coating. It is well established in the literature that the pure TMD coatings (especially WS₂) display excellent sliding properties in dry atmospheres. This means that in the absence of the moisture, the sliding is entirely of the TMDs. WSN5 and WSN12.5 coatings display similar friction properties and less value than the WSN20 due to the presence of strong (002) peaks. Here, it should be noted that the presence of some planes oriented in (100) direction did not affect the sliding properties of WSN5 coating as they did in other atmospheres. A minor increment in values from ~0.02 to ~0.03 as compared to the WS_x coating can be due to the presence of hard nitride particles. Finally, the highest COF of the WSN20 coating is due to its amorphous nature caused by the high N concentration. Amorphousness means no (002) planes thus, needing more time for alignment/tribolayer formation. Anyways, for the first time among all atmospheres, WSN20 coating displays highly stable frictional curves. In the dry N₂ tests, the reasons for the highest specific wear rates and exfoliation of the pure coating are same as discussed previously for other atmospheres. With N increments, increase in specific wear rates with increasing N content is observed. WSN20 coating displays highest wear rate

among the W–S–N coatings. This is again due to highest amount of hard nitride particles promoting abrasion and the amorphous nature of the coating. As said before, higher amorphousness means higher time and wear required for the tribolayer formation.

4.3. Brief comparison with W–S–C coatings

This section presents a brief comparison of the W–S–N coatings discussed above with the recently optimized W–S–C coatings deposited by our group. Initially, in a study, the W–S–C coatings were deposited by reactive sputtering, non-reactive sputtering of separate WS_2 and C targets and composite target sputtering. The analysis showed that the co-sputtered coatings display superior properties than the others [33]. Later, co-sputtering in a semi-industrial chamber was performed and the properties were optimized as a first step for developing coatings for 3D parts [28]. The maximum hardness achieved for the optimized W–S–C coatings was in the range of 5–7 GPa. Tribological tests were performed in atmospheres similar to this study. In room temperature, COF was 0.1–0.15 while, specific wear rate was in the range of $\sim 10^{-7}$. The shift to 200 °C resulted in a decrease of COF to 0.02–0.04 with same specific wear rate as of room temperature. Finally, the W–S–C coatings display COF of ~ 0.04 and specific wear rate in the $\sim 10^{-8}$ range, when tested in dry N_2 . The achieved properties are almost similar to what we observed for the W–S–N coatings.

The idea of this comparison is to show that the W–S–N coatings can efficiently suffice the need for an industrial system by replacing the W–S–C system when reactive sputtering becomes a need. Here comes another glitch that there are some cases where W–S–C coating deposition by co-sputtering is not preferred by the industries. So, in such cases the W–S–N coatings become the promising option as the achieved properties are very much replication of the W–S–C properties. This study is expected to promote the implementation of alloyed-TMDs in the industries.

5. Conclusions

In the present study, pure and N-alloyed WS_2 coatings are explored and compared with the W–S–C coatings. The main aim of this study is to explore the future of N-alloyed WS_2 coatings for the industries that prefer reactive sputtering over the conventional multiple targets sputtering process. For this purpose, a systematic study is performed with respect to the sliding properties of W–S–N coatings in different environments. To achieve good sliding properties, first step was to optimize the composition, morphology, structure and mechanical properties. The reference coating (WS_x) is stoichiometric with respect to WS_2 . N introduction in the chamber result in coatings with N content in the range of 14–26 at %. The pure WS_x coating is compact as compared to literature but display slight porosity when compared to the W–S–N coatings. Compactness increased and porosity decreased with increasing the N content. WS_x has a (100) preferential orientation which changed to (002) with the addition of N. Highest N-alloyed coating display an

amorphous XRD pattern. This (002) preferential orientation induces superior tribological properties in the coatings. The coatings display good adhesion to the substrates and excellent hardness. The pure WS_x coating has a hardness of 3.7 GPa while after N-alloying, a maximum hardness of 8.0 GPa is achieved, which is very comparable to the other works.

For the tribological tests, three different atmospheres are selected: room temperature, 200 °C and dry N_2 . It is well established in literature that the W–S–C coatings have the capability to display self-adaptive low friction properties in diverse atmospheres. However, the reactive sputtering is preferred by industries. So, it was very important that the W–S–N system is thoroughly investigated. The minimum friction coefficient and wear rates observed in room temperature, 200 °C and dry N_2 are 0.09 vs. $7.2 \times 10^{-8} \text{ mm}^3/\text{Nm}$, 0.02 vs. $7.1 \times 10^{-8} \text{ mm}^3/\text{Nm}$ and 0.03 vs. $9.3 \times 10^{-9} \text{ mm}^3/\text{Nm}$, respectively. The coatings presented in the current work are briefly compared with our recently optimized W–S–C coatings. It is shown that the composition, morphology, mechanical, friction and wear properties of W–S–N coatings are similar to W–S–C coatings. Moreover, their structural properties are even superior than W–S–C in some cases. So, this study communicates that there is quite high potential in W–S–N coatings for the industries which prefer reactive sputtering and want to avoid the adverse effects of hydrogen while using carbon containing carrier gases (CH_4 , C_2H_2).

Declaration of Competing Interest

The authors declare that they have no known competing financial interests or personal relationships that could have appeared to influence the work reported in this paper.

Acknowledgements

This work is sponsored by FEDER National funds FCT under the projects: SMARTLUB ref. "POCI-01-0145-FEDER-031807", ON-SURF ref. "POCI-01-0247-FEDER-024521", Atrito-0 ref. "POCI-01-0145-FEDER-030446", CEMMPRE ref. "UIDB/00285/2020" and "LA/P/0112/2020".

Appendix A. Supplementary data

Supplementary data to this article can be found online at <https://doi.org/10.1016/j.jmrt.2022.02.116>.

REFERENCES

- [1] Polcar T, Cavaleiro A. Review on self-lubricant transition metal dichalcogenide nanocomposite coatings alloyed with carbon. Surf Coating Technol 2011;206:686–95. <https://doi.org/10.1016/j.surfcoat.2011.03.004>.
- [2] Hilton MR. Fracture in MoS_2 solid lubricant films. Surf Coating Technol 1994;68–69:407–15. [https://doi.org/10.1016/0257-8972\(94\)90194-5](https://doi.org/10.1016/0257-8972(94)90194-5).

- [3] Donnet C, Erdemir A. Historical developments and new trends in tribological and solid lubricant coatings. *Surf Coating Technol* 2004;18:76–84. <https://doi.org/10.1016/j.surfcoat.2003.10.022>.
- [4] Roberts EW. Thin solid lubricant films in space. *Tribol Int* 1990;23:95–104. [https://doi.org/10.1016/0301-679X\(90\)90042-N](https://doi.org/10.1016/0301-679X(90)90042-N).
- [5] Scharf TW, Prasad SV. Solid lubricants: a review. *J Mater Sci* 2013;48:511–31. <https://doi.org/10.1007/s10853-012-7038-2>.
- [6] Voevodin AA, O'Neill JP, Prasad SV, Zabinski JS. Nanocrystalline WC and WC/a-C composite coatings produced from intersected plasma fluxes at low deposition temperatures. *J Vac Sci Technol A Vacuum, Surfaces, Film*. 1999;17:986–92. <https://doi.org/10.1116/1.581674>.
- [7] Voevodin AA, Neill JPO, Zabinski JS. WC/DLC/WS₂ nanocomposite coatings for aerospace tribology. *Tribol Lett* 1999;6:75–8.
- [8] Renevier NMU, Hampshire J, Fox VC, Witts J, Allen T, Teer DG. Advantages of using self-lubricating, hard, wear-resistant MoS₂-based coatings. *Surf Coating Technol* 2001;67–77. [https://doi.org/10.1016/S0257-8972\(01\)01108-2](https://doi.org/10.1016/S0257-8972(01)01108-2).
- [9] Savan A, Simmonds MC, Huang Y, Constable CP. Effects of temperature on the chemistry and tribology of co-sputtered MoS_x-Ti composite thin films. *Thin Solid Films* 2007;489:137–44. <https://doi.org/10.1016/j.tsf.2005.04.078>.
- [10] Scharf TW, Rajendran A, Banerjee R, Sequeda F. Growth, structure and friction behavior of titanium doped tungsten disulphide (Ti-WS₂) nanocomposite thin films. *Thin Solid Films* 2009;517:5666–75. <https://doi.org/10.1016/j.tsf.2009.02.103>.
- [11] Ding XZ, Zeng XT, He XY, Chen Z. Tribological properties of Cr- and Ti-doped MoS₂ composite coatings under different humidity atmosphere. *Surf Coating Technol* 2010;205:224–31. <https://doi.org/10.1016/j.surfcoat.2010.06.041>.
- [12] Bülbül F, Efeoğlu İ. Synergistic effect of bias and target currents for magnetron sputtered MoS₂-Ti composite films. *Mater. Test.* 2016;58:471–4. <https://doi.org/10.3139/120.110870>.
- [13] Qin X, Ke P, Wang A, Kim KH. Microstructure, mechanical and tribological behaviors of MoS₂-Ti composite coatings deposited by a hybrid HIPIMS method. *Surf Coating Technol* 2013;228:275–81. <https://doi.org/10.1016/j.surfcoat.2013.04.040>.
- [14] Rigato V, Maggioni G, Patelli A, Boscarino D, Renevier NM, Teer DG. Properties of sputter-deposited MoS₂/metal composite coatings deposited by closed field unbalanced magnetron sputter ion plating. *Surf Coating Technol* 2000;131:206–10. [https://doi.org/10.1016/S0257-8972\(00\)00797-0](https://doi.org/10.1016/S0257-8972(00)00797-0).
- [15] Mikhailov S, Savan A, Pflüger E, Knoblauch L, Hauert R, Simmonds M, et al. Morphology and tribological properties of metal (oxide)-MoS₂ nanostructured multilayer coatings. *Surf Coating Technol* 1998;105:175–83. [https://doi.org/10.1016/S0257-8972\(98\)00483-6](https://doi.org/10.1016/S0257-8972(98)00483-6).
- [16] Chien H, Ma K, Vattikuti SVP, Kuo C, Huo C, Chao C. Tribological behaviour of MoS₂/Au coatings. *Thin Solid Films* 2010;518:7532–4. <https://doi.org/10.1016/j.tsf.2010.05.040>.
- [17] Lince JR. Tribology of co-sputtered nanocomposite Au/MoS₂ solid lubricant films over a wide contact stress range. *Tribol Lett* 2004;17:419–28. <https://doi.org/10.1023/B:TRIL.0000044490.03462.6e>.
- [18] Zabinski JS, Donley MS, Walck SD, Schneider TR, McDevitt NT. The effects of dopants on the chemistry and tribology of sputter-deposited MoS₂ films. *Tribol Trans* 1995;38:894–904. <https://doi.org/10.1080/10402009508983486>.
- [19] Li H, Zhang G, Wang L. Low humidity-sensitivity of MoS₂/Pb nanocomposite coatings. *Wear* 2016;350–351:1–9. <https://doi.org/10.1016/j.wear.2015.12.008>.
- [20] Simmonds MC, Savan A, Pflüger E, Van Swygenhoven H. Mechanical and tribological performance of MoS₂ co-sputtered composites. *Surf Coating Technol* 2000;126:15–24. [https://doi.org/10.1016/S0257-8972\(00\)00521-1](https://doi.org/10.1016/S0257-8972(00)00521-1).
- [21] Kao WH. Tribological properties and high speed drilling application of MoS₂-Cr coatings. *Wear* 2005;258:812–25. <https://doi.org/10.1016/j.wear.2004.09.045>.
- [22] Jianxin D, Wenlong S, Hui Z, Jinlong Z. Performance of PVD MoS₂/Zr-coated carbide in cutting processes. *Int J Mach Tool Manufact* 2008;48:1546–52. <https://doi.org/10.1016/j.ijmachtools.2008.06.009>.
- [23] Ye M, Zhang G, Ba Y, Wang T, Wang X, Liu Z. Microstructure and tribological properties of MoS₂ + Zr composite coatings in high humidity environment. *Appl Surf Sci* 2016;367:140–6. <https://doi.org/10.1016/j.apsusc.2016.01.163>.
- [24] Nainaparampil JJ, Phani AR, Krzanowski JE, Zabinski JS. Pulsed laser-ablated MoS₂-Al films: friction and wear in humid conditions. *Surf Coating Technol* 2004;187:326–35. <https://doi.org/10.1016/j.surfcoat.2004.02.043>.
- [25] Polcar T, Cavaleiro A. Self-adaptive low friction coatings based on transition metal dichalcogenides. *Thin Solid Films* 2011;519:4037–44. <https://doi.org/10.1016/j.tsf.2011.01.180>.
- [26] Hudec T, Mikula M, Satrapinskyy L, Roch T, Truchlý M, Švec Jr P, et al. Structure, mechanical and tribological properties of Mo-S-N solid lubricant coatings. *Appl Surf Sci* 2019;486:1–14. <https://doi.org/10.1016/j.apsusc.2019.03.294>.
- [27] Hudec T, Roch T, Gregor M, Orovčík Ľ, Mikula M, Polcar T. Tribological behaviour of Mo-S-N solid lubricant coatings in vacuum, nitrogen gas and elevated temperatures. *Surf Coating Technol* 2020;126722. <https://doi.org/10.1016/j.surfcoat.2020.126722>.
- [28] Vuchkov T, Evaristo M, Bin Yaquib T, Cavaleiro A. The effect of substrate location on the composition, microstructure and mechano-tribological properties of W-S-C coatings deposited by magnetron sputtering. *Surf Coating Technol* 2020;386:125481. <https://doi.org/10.1016/j.surfcoat.2020.125481>.
- [29] Vuchkov T, Evaristo M, Bin Yaquib T, Polcar T, Cavaleiro A. Synthesis, microstructure and mechanical properties of W-S-C self-lubricant thin films deposited by magnetron sputtering. *Tribol Int* 2020;150:106363. <https://doi.org/10.1016/j.triboint.2020.106363>.
- [30] Bin Yaquib T, Bruyere S, Pierson JF, Vuchkov T, Cavaleiro A. Insights into the wear track evolution with sliding cycles of carbon-alloyed transition metal dichalcogenide coatings. *Surf Coating Technol* 2020;403:126360. <https://doi.org/10.1016/j.surfcoat.2020.126360>.
- [31] Bin Yaquib T, Vuchkov T, Sanguino P, Polcar T, Cavaleiro A. Comparative study of DC and RF sputtered MoSe₂ coatings containing carbon—an approach to optimize stoichiometry, microstructure, crystallinity and hardness. *Coatings* 2020;10:133. <https://doi.org/10.3390/coatings10020133>.
- [32] Kannur KH, Bin Yaquib T, Huminiuc T, Polcar T, Pupier C, Héau C, et al. Synthesis and structural properties of Mo-S-N sputtered coatings. *Appl Surf Sci* 2020;527:146790. <https://doi.org/10.1016/j.apsusc.2020.146790>.
- [33] Vuchkov T, Bin Yaquib T, Evaristo M, Cavaleiro A. Synthesis, microstructural, and mechano-tribological properties of self-lubricating W-s-C(H) thin films deposited by different RF magnetron sputtering procedures. *Coatings* 2020;10. <https://doi.org/10.3390/coatings10030272>.
- [34] Bin Yaquib T, Vuchkov T, Evaristo M, Cavaleiro A. DCMS Mo-Se-C solid lubricant coatings – synthesis, structural, mechanical and tribological property investigation. *Surf Coating Technol* 2019. <https://doi.org/10.1016/j.surfcoat.2019.124992>.
- [35] Bin Yaquib T, Hebbar Kannur K, Vuchkov T, Pupier C, Héau C, Cavaleiro A. Molybdenum diselenide coatings as universal

- dry lubricants for terrestrial and aerospace applications. *Mater Lett* 2020;275:128035. <https://doi.org/10.1016/j.matlet.2020.128035>.
- [36] Cao H, Wen F, Kumar S, Rudolf P, De Hosson JTM, Pei Y. On the S/W stoichiometry and triboperformance of WSxC(H) coatings deposited by magnetron sputtering. *Surf Coating Technol* 2018. <https://doi.org/10.1016/J.SURFCOAT.2018.04.040>.
- [37] Nossa A, Cavaleiro A. Mechanical behaviour of W-S-N and W-S-C sputtered coatings deposited with a Ti interlayer. *Surf Coating Technol* 2003;163–164:552–60. [https://doi.org/10.1016/S0257-8972\(02\)00622-9](https://doi.org/10.1016/S0257-8972(02)00622-9).
- [38] Takeno T, Abe S, Adachi K, Miki H, Takagi T. Deposition and structural analyses of molybdenum-disulfide (MoS₂)-amorphous hydrogenated carbon (a-C:H) composite coatings. *Diam Relat Mater* 2010;19:548–52. <https://doi.org/10.1016/j.diamond.2009.10.028>.
- [39] Wu Y, Li H, Ji L, Liu L, Ye Y, Chen J, et al. Structure, mechanical, and tribological properties of MoS₂/a-C:H composite films. *Tribol Lett* 2013;52:371–80. <https://doi.org/10.1007/s11249-013-0216-9>.
- [40] Wu Y, Li H, Ji L, Ye Y, Chen J, Zhou H. A long-lifetime MoS₂/a-C:H nanoscale multilayer film with extremely low internal stress. *Surf Coating Technol* 2013;236:438–43. <https://doi.org/10.1016/j.surfcoat.2013.10.021>.
- [41] Nossa A, Cavaleiro A. The influence of the addition of C and N on the wear behaviour of W-S-C/N coatings. *Surf Coating Technol* 2001;142–144:984–91. [https://doi.org/10.1016/S0257-8972\(01\)01249-X](https://doi.org/10.1016/S0257-8972(01)01249-X).
- [42] Nossa A, Cavaleiro A, Carvalho NJM, Kooi BJ, De Hosson JTM. On the microstructure of tungsten disulfide films alloyed with carbon and nitrogen. *Thin Solid Films* 2005;484:389–95. <https://doi.org/10.1016/j.tsf.2005.02.018>.
- [43] Tomastik C, Tomala A, Pauschitz A, Roy M. The influence of carbon content on the microtribological performance of W-S-C films. *J. Eng. Tribol.* 2014;228:745–55. <https://doi.org/10.1177/1350650114529753>.
- [44] Hebbar K, Huminiuc T, Bin T, Polcar T, Pupier C, Christophe H, et al. In: An insight on the MoS₂ tribo-film formation to determine the friction performance of Mo-S-N sputtered coatings, vol. 408; 2021. <https://doi.org/10.1016/j.surfcoat.2020.126791>.
- [45] Nossa A, Cavaleiro A. Behaviour of nanocomposite coatings of W-S-N/C system under pin -on-Disk Testing 2004;456:515–9. <https://doi.org/10.4028/www.scientific.net/MSF.455-456.515>.
- [46] Nossa A, Cavaleiro A. Chemical and physical characterization of C(N)-doped W-S sputtered films. *J Mater Res* 2004;19:2356–65. <https://doi.org/10.1557/JMR.2004.0293>.
- [47] Nossa A, Cavaleiro A. Tribological behaviour of N(C)-alloyed W-S films. *Tribol Lett* 2007;28:59–70. <https://doi.org/10.1007/s11249-007-9248-3>.
- [48] Gustavsson F, Jacobson S, Cavaleiro A, Polcar T. Ultra-low friction W-S-N solid lubricant coating. *Surf Coating Technol* 2013;232:541–8. <https://doi.org/10.1016/j.surfcoat.2013.06.026>.
- [49] Sundberg J, Nyberg H, Särhammar E, Nyberg T, Jacobson S, Jansson U. Influence of composition, structure and testing atmosphere on the tribological performance of W-S-N coatings. *Surf Coating Technol* 2014;258:86–94. <https://doi.org/10.1016/j.surfcoat.2014.09.061>.
- [50] Isaeva L, Sundberg J, Mukherjee S, Pelliccione CJ, Lindblad A, Segre CU, et al. Amorphous W-S-N thin films: the atomic structure behind ultra-low friction. *Acta Mater* 2015;82:84–93. <https://doi.org/10.1016/j.actamat.2014.08.043>.
- [51] Zhu J, Zeng Q, Zhang B, Yan C, He W. Elevated-temperature super-lubrication performance analysis of dispersion-strengthened WSN coatings : experimental research and first-principles calculation. *Surf Coating Technol* 2021;406:126651. <https://doi.org/10.1016/j.surfcoat.2020.126651>.
- [52] Mutafov P, Evaristo M, Cavaleiro A, Polcar T. Structure, mechanical and tribological properties of self-lubricant W-S-N coatings. *Surf Coating Technol* 2015;261:7–14. <https://doi.org/10.1016/j.surfcoat.2014.11.074>.
- [53] Liu H, Zhang X. Improved tribological properties of sputtered MoS₂ films through N⁺ implantation. *Thin Solid Films* 1994;240:97–100. [https://doi.org/10.1016/0040-6090\(94\)90702-1](https://doi.org/10.1016/0040-6090(94)90702-1).
- [54] Zhang X, Qiao L, Chai L, Xu J, Shi L, Wang P. Structural, mechanical and tribological properties of Mo-S-N solid lubricant films. *Surf Coating Technol* 2016;296:185–91. <https://doi.org/10.1016/j.surfcoat.2016.04.040>.
- [55] Oliver WC, Pharr GM. An improved technique for determining hardness and elastic modulus using load and displacement sensing indentation experiments. *J Mater Res* 1992. <https://doi.org/10.1557/JMR.1992.1564>.
- [56] Contacts S, Encounters M. In: Contact and rubbing of flat surfaces, vol. 981; 2004. <https://doi.org/10.1063/1.1721448>.
- [57] Xu S, Sun J, Weng L, Hua Y, Liu W, Neville A, et al. In-situ friction and wear responses of WS₂ films to space environment : vacuum and atomic oxygen. *Appl Surf Sci* 2018;447:368–73. <https://doi.org/10.1016/j.apsusc.2018.04.012>.
- [58] Weise G, Mattern N, Hermann H, Teresiak A, Bächer I, Brückner W, et al. Preparation, structure and properties of MoS_x films. *Thin Solid Films* 1997;298:98–106. [https://doi.org/10.1016/S0040-6090\(96\)09165-1](https://doi.org/10.1016/S0040-6090(96)09165-1).
- [59] Cavaleiro A, Kannur KH, Bin Yaqub T, Pupier C, He C. Mechanical properties and vacuum tribological performance of Mo – S – N sputtered coatings. *ACS Appl Mater Interfaces* 2020. <https://doi.org/10.1021/acsami.0c12655>.
- [60] Cao H, De Hosson JTM, Pei Y. Effect of carbon concentration and argon flow rate on the microstructure and triboperformance of magnetron sputtered WS₂/a-C coatings. *Surf Coating Technol* 2017;332:142–52. <https://doi.org/10.1016/j.surfcoat.2017.06.087>.
- [61] Leyland A, Matthews A. On the significance of the H/E ratio in wear control: a nanocomposite coating approach to optimised tribological behaviour. *Wear* 2000;246:1–11. [https://doi.org/10.1016/S0043-1648\(00\)00488-9](https://doi.org/10.1016/S0043-1648(00)00488-9).
- [62] Musil J, Kunc F, Zeman H, Poláková H. Relationships between hardness, Young's modulus and elastic recovery in hard nanocomposite coatings. *Surf Coating Technol* 2002;154:304–13. [https://doi.org/10.1016/S0257-8972\(01\)01714-5](https://doi.org/10.1016/S0257-8972(01)01714-5).
- [63] Charitidis CA, Logothetidis S. Effects of normal load on nanotribological properties of sputtered carbon nitride films. *Diam Relat Mater* 2005;14:98–108. <https://doi.org/10.1016/j.diamond.2004.07.022>.
- [64] Martin PM. *Handbook of deposition technologies for films and coatings: science, applications and technology*. Elsevier; 2009.
- [65] Fernandes F, Yaqub TB, Cavaleiro A. Influence of Ag additions on the structure , mechanical properties and oxidation behaviour of Cr-O coatings deposited by HiPIMS. *Surf Coating Technol* 2018;339:167–80. <https://doi.org/10.1016/j.surfcoat.2018.02.025>.
- [66] Polcar T, Cavaleiro A. Self-adaptive low friction coatings based on transition metal dichalcogenides 2011;519:4037–44. <https://doi.org/10.1016/j.tsf.2011.01.180>.
- [67] Hudec T, Izai V, Satrapinskyy L, Huminiuc T, Roch T, Gregor M, et al. Structure, mechanical and tribological properties of MoSe₂ and Mo-Se-N solid lubricant coatings Tomás. *Surf Coating Technol* 2020;126536. <https://doi.org/10.1016/j.surfcoat.2020.126536>.
- [68] Muratore C, Voevodin AA. Control of molybdenum disulfide basal plane orientation during coating growth in pulsed magnetron sputtering discharges. *Thin Solid Films* 2009;517:5605–10. <https://doi.org/10.1016/j.tsf.2009.01.190>.

- [69] Rasamani KD, Alimohammadi F, Sun Y. Interlayer-expanded MoS₂, mater. Today Off 2017;20. <https://doi.org/10.1016/j.mattod.2016.10.004>.
- [70] Panigrahi PK, Pathak A. Aqueous medium synthesis route for randomly stacked molybdenum disulfide. J. Nanoparticles 2013. <https://doi.org/10.1155/2013/671214>.
- [71] Bin Yaqub T, Vuchkov T, Cavaleiro A. A revised interpretation of the mechanisms governing low friction tribolayer formation in alloyed-TMD self-lubricating coatings. Appl Surf Sci 2022;571. <https://doi.org/10.1016/j.apsusc.2021.151302>.
- [72] Pimentel JV, Danek M, Polcar T, Cavaleiro A. Effect of rough surface patterning on the tribology of W-S-Cr self-lubricant coatings. Tribol Int 2014;69:77–83. <https://doi.org/10.1016/j.triboint.2013.09.004>.
- [73] Polcar T, Evaristo M, Cavaleiro A. Self-lubricating W-S-C nanocomposite coatings, plasma process. Polymer 2009;6:417–24. <https://doi.org/10.1002/ppap.200930005>.
- [74] Polcar T, Evaristo M, Stueber M, Cavaleiro A. Mechanical and tribological properties of sputtered Mo-Se-C coatings. Wear 2009;266:393–7. <https://doi.org/10.1016/j.wear.2008.04.010>.
- [75] Kubart T, Polcar T, Kopecký L, Novák R, Nováková D. Temperature dependence of tribological properties of MoS₂ and MoSe₂ coatings. Surf Coating Technol 2005;193:230–3. <https://doi.org/10.1016/j.surfcoat.2004.08.146>.
- [76] Cao H, Wen F, Kumar S, Rudolf P, De Hosson JTM, Pei Y. On the S/W stoichiometry and triboperformance of WS_xC(H) coatings deposited by magnetron sputtering. Surf Coating Technol 2018. <https://doi.org/10.1016/j.surfcoat.2018.04.040>.
- [77] Cao H, Wen F, De Hosson JTM, Pei YT. Instant WS₂ platelets reorientation of self-adaptive WS₂/a-C tribocoating. Mater Lett 2018;229:64–7. <https://doi.org/10.1016/j.matlet.2018.06.111>.
- [78] Lancaster JK. A review of the influence of environmental humidity and water on friction, lubrication and wear. Tribol Int 1990;23:371–89. [https://doi.org/10.1016/0301-679X\(90\)90053-R](https://doi.org/10.1016/0301-679X(90)90053-R).
- [79] Waghray H, Lee T-S, Tatarchuk BJ. A study of the tribological and electrical properties of sputtered and burnished transition metal dichalcogenide films. Surf Coating Technol 1995;76–77:415–20. [https://doi.org/10.1016/0257-8972\(95\)02564-2](https://doi.org/10.1016/0257-8972(95)02564-2).
- [80] Hilton MR, Bauer R, Didzulis SV, Dugger MT, Keem JM, Scholhamer J. Structural and tribological studies of MoS₂ solid lubricant films having tailored metal-multilayer nanostructures. Surf Coating Technol 1992;53:13–23. [https://doi.org/10.1016/0257-8972\(92\)90099-V](https://doi.org/10.1016/0257-8972(92)90099-V).